Journal of Computers Vol. 35 No. 2, April 2024, pp. 151-166
doi: 10.53106/199115992024043502010

Research on Computer Aided Deformation Control Strategy for Welding of Large Long Straight Beams

Jian-Wei Qi[1], Dan-Dan Cui[2*]

[1] Tangshan Maritime Institute,
Tangshan City 063000, Hebei Province, China
jianwei5732@126.com

[2] Tangshan Polytechnic College,
Tangshan City 063000, Hebei Province, China
cuidandan2018@126.com

Received 27 March 2024; Revised 2 April 2024; Accepted 15 April 2024

Abstract. Long straight string beams are often used as supporting structures in large equipment. Due to the large size of string beams, welding technology is generally used to complete their production. This article first constructs the finite element model and heat source model of the chord beam based on the structure of the long straight beam, and then obtains the distribution and evolution law of the temperature field, as well as the temperature rise law of the temperature field under dynamic simulation. Based on this law data, an improved BP neural network model is used to predict the deformation of the beam. In order to verify the authenticity of the prediction results, the article finally builds a Matlab simulation experimental environment and conducts simulation experiments on the welding deformation prediction of the beam.

Keywords: long straight chord beam, welding deformation, BP neural network, finite element analysis

1 Introduction

Long straight string beams often appear in various load-bearing structures, such as bridge cranes, high-speed train carriages, or partial frame structures in subway tracks. As an important load-bearing support structure, the production quality of long straight chord beams has an undeniable impact on the reliability of the overall structure of the equipment [1].

However, the characteristic of this long and straight structure inevitably leads to residual welding stress during the production process of long beams due to local rapid heating and cooling caused by welding. This article takes the box type long straight chord beam used in high-speed trains as an example. This type of beam is a typical long chord beam structure with a large structural size and requires longer welding seams. Therefore, during the welding process, there is a large heat input, and after welding is completed, it is easy to produce axial bending deformation and overall twisting deformation. Therefore, controlling the welding deformation of the long straight chord beam is particularly important in the beam manufacturing process [2].

For the control of welding deformation, traditional production processes mainly rely on empirical methods, but empirical methods often do not have replicability. The new welding deformation control method is computer-aided. By combining computer-aided and intelligent algorithms, based on existing empirical data as a dataset, prediction of welding deformation with long straight chord beams can be achieved, thereby achieving deformation control during the welding process of chord beams. Therefore, the main work of this article is as follows:

1) Based on the characteristics of the target object being welded, this article first establishes the finite element and heat source models of the chord beam, which facilitates the analysis of the welding process.

2) Based on existing data, use an improved BP neural network to predict the welding process. Constructed a prediction model and improved the prediction process.

3) A simulation experiment model was built using Matlab simulation software, and the simulation experiment was completed. The predicted results were compared with the actual results, achieving the expected results.

* Corresponding Author

The chapter composition of this article is as follows: Chapter 2 summarizes the relevant research results of scholars, Chapter 3 mainly introduces the finite element analysis process and heat source analysis process of welding process, Chapter 4 uses finite element analysis method to construct neural network models on the basis of finite metadata, Chapter 5 mainly introduces the construction process of simulation experiments, and Chapter 6 is the conclusion section.

2 Related Works

In recent years, with the continuous improvement of welding mechanics theory and the rapid development of computer technology, digital simulation technology has become an effective tool for predicting and controlling welding deformation. In terms of predicting welding deformation, the mainstream technical method is the thermal elastic plastic finite element method [3], and scholars have conducted extensive research in the field of welding deformation research.

Bing Li conducted research on the welding deformation problem of the cabin skeleton structure, conducted welding tests on typical joints of the cabin skeleton, and established a thermal elastoplastic finite element model of local joints. The temperature field was numerically simulated, and the experimental simulation results were consistent with the actual welding experimental results, indicating the accuracy of the prediction [4].

Yuelai Zhang used the thermal elastoplastic finite element method and enhanced moving heat source model to numerically simulate the welding deformation of a large straight structure of locomotive and vehicle with a length of 13832 mm. Through the numerical model, the deformation of the crossbeam was predicted, which guided the actual production of large straight structures and shortened the process development cycle [5].

Xiaowei Pu calculated the welding residual stress of thick joints using both instantaneous and moving heat sources. The results showed that using instantaneous heat source calculation can significantly reduce calculation time and ensure high calculation accuracy [6].

Liu used isothermal compression tests to obtain flow stresses at different temperatures, strains, and strain rates, and used BP neural network technology to predict the anisotropic nonlinear thermodynamic parameters of materials. The predictions were in good agreement with experimental results, thus verifying the effectiveness of this method for nonlinear models [7].

Guangtao Zhou from Huaqiao University proposed a new method of flexible control of welding instability deformation of high-strength aluminum alloy thin plates using “welding high-speed airflow field” from a mechanical perspective. He studied the effective feasibility of this method in controlling the welding deformation of 2A12 high-strength aluminum alloy thin plates, analyzed the influence of welding high-speed airflow load on the stress evolution law of thin plates, and elucidated its control of welding residual stress and deformation mechanism. The control process and analysis process have guiding significance for welding materials in this article [8].

Hanlin Gao from the University of Mining and Technology mainly elaborated on an effective finite element analysis method, simulated and calculated the welding temperature field and residual stress field of the key weld seam of the support ear, and analyzed the influence of different welding sequences on residual stress and deformation. This method has great application value in the research of welding sequence welding thermal field [9].

3 Establishment of Finite Element Model for Long String Beam

The welding structure model of the chord beam is shown in Fig. 1, with a length of 2898 millimeters, a cross-sectional length of 373 millimeters, and a width of 147 millimeters. A steel plate with a thickness of 5 millimeters is selected for welding. The steel plate material is Q420D low alloy high-strength steel, and the internal steel structure metal is Q390D. The welding wire model for welding is CHW-55C1, and the chemical composition is shown in Table 1. The chemical composition of internal steel Q390D is shown in Table 2. The chemical composition of the welding rod is shown in Table 3. The welding grooves of the welds on the beam are all 55 ° HY shaped grooves, and the experiment uses melting electrode active gas shielded welding. The welding process parameters are shown in Table 4.

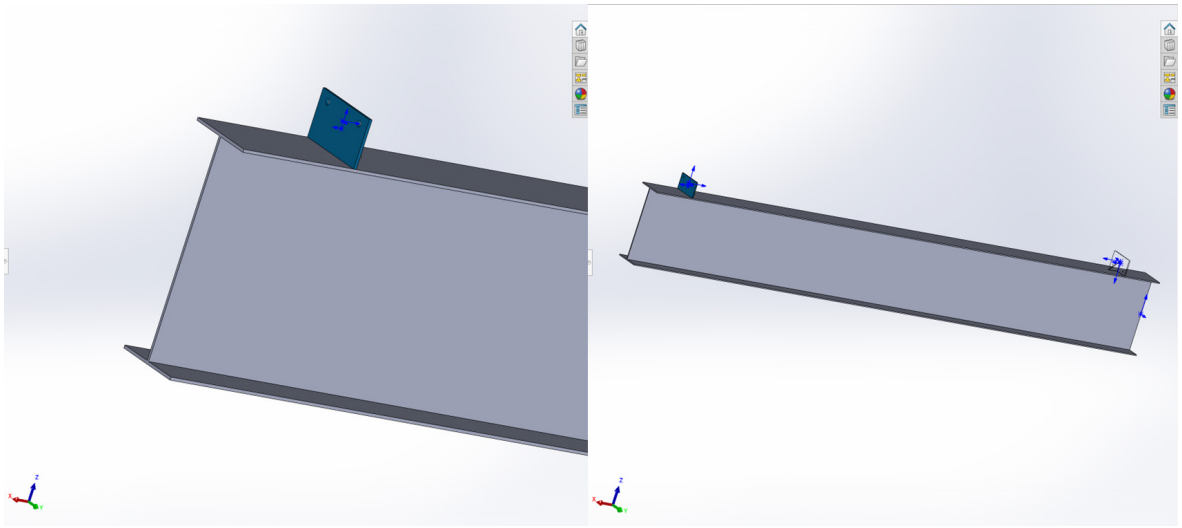

Fig. 1. Schematic diagram of beam structure

Table 1. Chemical composition of Q420D low alloy high-strength steel

C (%)	Mn (%)	Si (%)	P (%)	S (%)	V (%)
0.2	1-1.7	0.55	0.03	0.03	0.02-0.20
Nb (%)	Ti (%)	Al (%)	Cr (%)	Ni (%)	
0.02	0.2	0.15	0.4	0.7	

Table 2. Chemical composition of Q390D low alloy high-strength steel

C (%)	Mn (%)	Si (%)	P (%)	S (%)	V (%)
0.2	1-1.6	0.55	0.03	0.03	0.02-0.20
Nb (%)	Ti (%)	Al (%)	Cr (%)	Ni (%)	
0.06	0.2	0.15	0.3	0.7	

Table 3. Chemical composition of CHW-55C1 welding wire

C (%)	Mn (%)	Si (%)	P (%)	S (%)	Mo (%)	Fe (%)	Cr (%)	Ni (%)
0.2	1.06	0.53	0.01	0.01	0.12	0.15	0.01	0.93

Table 4. Welding process parameters

Gas flow rate Q/ ($L \cdot \min^{-1}$)	Welding current I / A	Arc voltage U / A	Welding speed v / ($mm \cdot s^{-1}$)
22	270	31	14.6

The temperature changes, material composition, and cooling process during the welding process can all lead to different welding results. Therefore, before establishing finite element analysis, it is necessary to treat the cross results of the physical and chemical phenomena involved in the welding material, including heat transfer process, material melting and solidification, metallographic phase transformation, stress and deformation, as variable conditions. However, in the actual welding process, various factors change complex. In order to increase convergence, appropriate simplification treatment is adopted for individual links in the model to improve calculation efficiency.

The changes in metal materials caused by welding heat and the residual stress changes in various welding parts, as well as the mutual influence relationship between thermal field, force field, and metallographic structure, are shown in Fig. 2. The solid line indicates a significant impact relationship, while the dashed line indicates a relatively weak impact relationship [10].

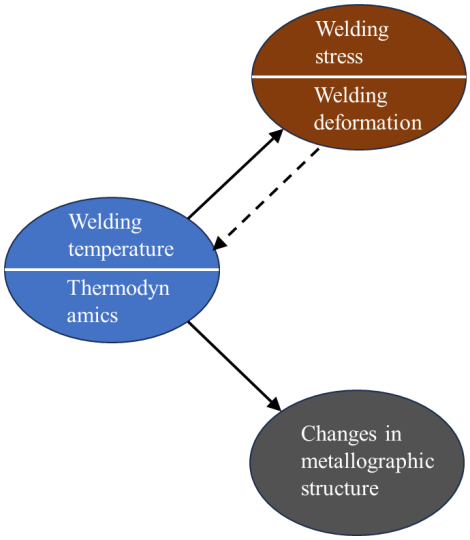

Fig. 2. The mutual influence relationship between various factors

3.1 Finite Element Analysis Mechanism of Welding Process

The variation of temperature field during the welding process is the main factor determining the residual stress and welding deformation of the welded workpiece. Welding process parameters, metal thermophysical properties, and heat source model size are all key factors. During the welding process, rapid heating and cooling occur. With the movement of the heat source, a significant temperature gradient is generated at the weld seam of the specimen, causing changes in the material's properties. Therefore, welding is a nonlinear transient process, and the heat conduction control equation for the welding process is [11]:

$$\overline{Q} = \rho C \frac{\partial T}{\partial t} - \frac{\partial\left(\frac{\partial T}{\partial x}\right)}{\partial x} - \frac{\partial\left(\frac{\partial T}{\partial y}\right)}{\partial y} - \frac{\partial\left(\frac{\partial T}{\partial z}\right)}{\partial z}. \tag{1}$$

ρ - The density of the welding material;
C - Specific heat capacity of welding materials;
T - Temperature field distribution function;
t - Heat transfer time;
λ - The thermal conductivity of the material;
$\overline{Q}$ - Internal heat source intensity.

To solve Formula 1, it is necessary to determine the boundary conditions and initial conditions for welding. In this article, the environmental temperature and the initial temperature of the component are taken into account.

As the initial condition, the heat loss on the surface of the component is taken as the boundary condition, and the expression of the boundary condition is:

$$\begin{aligned}&\beta\frac{\partial T}{\partial x}\cos\theta_x+\beta\frac{\partial T}{\partial y}\cos\theta_y+\\&\beta\frac{\partial T}{\partial z}\cos\theta_z-q_s(x,y,z,t)=0.\end{aligned}\tag{2}$$

$\cos\theta_x$, $\cos\theta_y$, $\cos\theta_z$ - the cosine value of the boundary normal direction;
T - is the temperature on the known boundary;
q_s - is the external input heat source per unit area;
β - is the heat transfer coefficient of the beam surface.

The finite element analysis of temperature field is a three-dimensional nonlinear transient heat conduction analysis, which first divides the overall spatial domain into grids, discretizes the spatial domain, and then calculates it using the finite element method. The time domain is calculated using the finite difference method.

The temperature of nodes within each unit is represented as:

$$T=[N]^e\{T\}^e.\tag{3}$$

$[N]^e$ - Shape function;
$\{T\}^e$ - Unit node temperature;

The above formula is weighted and the processed formula is represented as:

$$[K]\{T\}+[C]\frac{\partial\{T\}}{\partial t}=\{Q\}.\tag{4}$$

$[K]$ - Temperature variation matrix during welding process, represented by:

$$[K]=\sum\left([K_1]^e+[K_2]^e\right).\tag{5}$$

$\{T\}$- is the column vector of node temperature;
$[C]$ - is the heat capacity matrix; The representation method is:

$$[C]=\sum[C]^e.\tag{6}$$

$\{Q\}$- is the node heat flux vector. The representation method is:

$$[Q]=\sum\left(\{Q_1\}^e+\{Q_2\}^e\right).\tag{7}$$

Discretize the time domain using the weighted difference method, taking the time interval A and the temperature and boundary conditions in the spatial domain C at time B are known. The discretization equation is:

$$\frac{\{T_{n-1}\}-\{T_n\}}{\Delta t}=\delta\left(\frac{\partial\{T_{n-1}\}}{\partial t}-\frac{\partial\{T_n\}}{\partial t}\right).\tag{8}$$

δ - is the weighting coefficient, $\theta \in [0,1]$.

Further organizing formulas 4 and 8, the following calculations can be obtained:

$$\left[\frac{[C]}{\Delta t}+\delta[K]\right]\{T\}-\left[\delta\{Q_n\}+(1-\delta)\{Q_{n-1}\}\right] = \left[\frac{[C]}{\Delta t}+(\delta-1)[T]\right]. \tag{9}$$

Given the initial temperature matrix, the temperature distribution in the spatial domain can be derived at any time, and different difference schemes can be obtained based on different weighting coefficient values:

$\delta = 0$, the differential format is backward differential;

$\delta = 0.5$, the differential format is centered differential;

$\delta = 1$ the differential format is forward differential.

3.2 Establishment of Finite Element Model

The welding process is quite complex, and in the process of finite element analysis, the influence of secondary effects on the welding process should be ignored according to the research focus. Therefore, while ensuring calculation accuracy, the finite element analysis of the welding process will simplify the model as follows:

(1) The specimens used in this experiment were welded using carbon dioxide gas shielded welding, with the welding rod model CHW-55C1. To ensure the stability of welding metal fusion, it is assumed that the properties and physical properties of the welding wire and the welding object are consistent;

(2) The specimens used in this study were processed in a common machining workshop in northern China, so the initial average temperature for finite element simulation is assumed to be 20 °C;

(3) During the welding process, heat exchange occurs between the specimen and the environment through thermal convection and radiation existing on the surface of the specimen;

(4) The welding process of the specimen in this article adopts double-sided multi pass welding. The fusion zone is formed between the weld and the base metal due to high-temperature melting, and the size and shape of the fusion zone are relatively regular. To facilitate modeling and improve computational efficiency, it is assumed that the weld is of a regular geometric shape;

(5) Not considering metal phase transition and heat transfer of fluid metal inside the weld pool.

The welding groove form of the beam and the welded components on the beam is shown in Fig. 3.

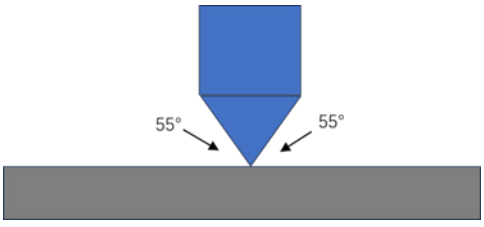

Fig. 3. Weld joint groove form

To accurately calculate the welding deformation of the chord beam, it is necessary to establish a three-dimensional finite element mesh model that is exactly the same as the actual structural dimensions. In the actual welding process, due to the complexity of the welding process and the diversity of welding temperature changes, it is not possible to quantitatively describe the welding of beams. Therefore, corresponding simplification measures need to be taken when establishing the model: ignoring the flow process of the molten pool, welding solidification process and phase transformation process, and ignoring the influence of welding deformation on the welding thermal field [12]. To improve computational efficiency and ensure the accuracy of simulation results, local re-

finement of the grid is carried out at the positions of the weld and heat affected zone, with a minimum grid size of 6.45 mm. The grid away from the weld area is coarsened, and the maximum grid size reaches 22.7 mm. The grid division result is shown in Fig. 4, with a total of 14117 nodes and 71408 solid units.

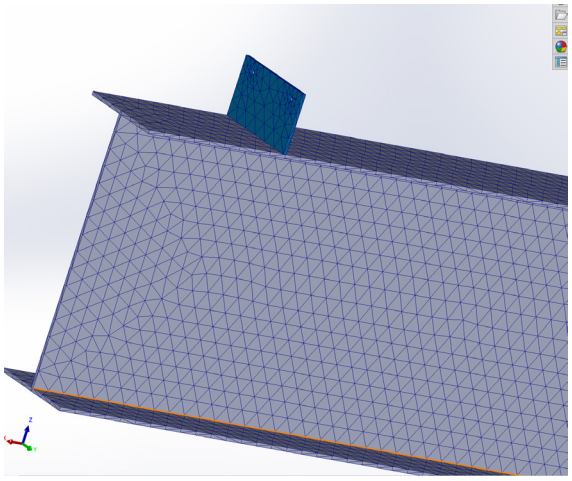

Fig. 4. The mesh division results of the three-dimensional model of the beam

3.3 Establishment of Heat Source Model

Before establishing a heat source model, the first step is to determine the thermal conductivity, density, and specific heat capacity of the material at different temperatures. From the relevant research results in China, the data on the thermal physical properties of materials at high temperatures is not comprehensive, and there is a lack of research on the thermal physical properties of materials near the melting point temperature. After plastic strain occurs, the properties of materials are also difficult to predict. As shown in Fig. 5, the thermal physical properties of Q390D and Q420D are used to set the boundary conditions for welding. The brown color in the picture represents Q390D, and the green color represents Q420D.

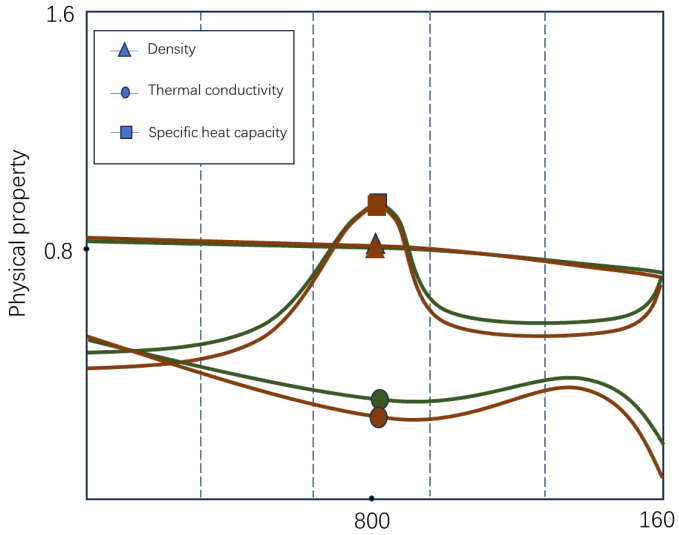

Fig. 5. The relationship between material physical properties and temperature

The welding of the beam is completed in the factory, which is located in northern China with dry and distinct climate conditions. Therefore, the initial average temperature set for finite element simulation is 20 ℃, and the ambient temperature is set to 20 ℃, taking into account both thermal convection and radiation between the surface of the specimen and the environment., The absolute zero temperature is -273.15 ℃, and the convective heat transfer coefficient is set to $15W / m^2 \cdot$℃ and the thermal radiation coefficient is set to 0.7, further establishing a Gaussian heat source model.

During the welding process, the heat is mainly applied to the weld seam area, while considering the role of the heat source in the vicinity of the heat affected zone. Considering that the influence of the arc is relatively small in the welding process of large beams, a Gaussian heat source [13] model is established as shown in Fig. 6.

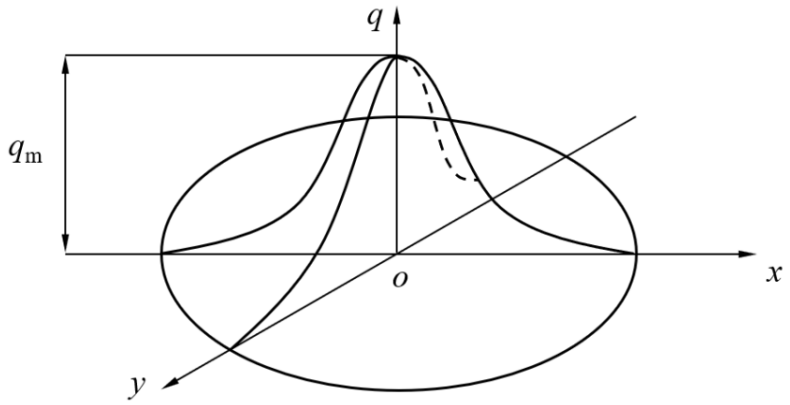

Fig. 6. Gaussian heat source model

The heat flux density at any point within the loading range of a Gaussian heat source can be expressed using the following formula:

$$h\left(R\right) = h_m \exp\left(-\frac{3R^2}{r^2}\right). \tag{10}$$

Among them, h_m is the heat flux density, expressed as:

$$h_m = \frac{3}{\pi r^2} Q. \tag{11}$$

$$Q = \phi U_h I_h. \tag{12}$$

R - The distance from the point to the center of the heat source;
r - Heating radius of the arc;
Q - Heat source energy;
ϕ - Welding thermal efficiency;
U_h - Welding voltage;
I_h - Welding current.

According to the above process, based on the variable length heat source and instantaneous heat source, dynamic simulation methods were used to complete the dynamic simulation of the heating of the chord beam. Through the analysis of the key path and key point temperatures, the distribution and evolution laws of the tem-

perature field under the dynamic simulation of the chord beam, as well as the temperature rise laws of the temperature field under the dynamic simulation, were obtained [14].

When the chord beam material in this article is heated in a certain time step, assuming that the main temperature rise area is on the X3-X8 node area (where X = A, B, C, D, ...), and the other nodes are all at ambient temperature, then when conducting the heating calculation in the next time step, it is necessary to step the temperature of X3-X8 node into a unit grid distance along the production direction of the beam, that is, assign the temperature of X3-X8 node to the temperature of X4-X9 node, and set the temperature of X3 node as ambient temperature, which is used as the initial temperature load for the next time step for calculation.

The specific factual process of dynamic heating simulation is as follows:

(1) Create a finite element analysis case file in SolidWorks Simulation based on the number of temperature nodes in the "Y" - shaped region to be combined.

(2) Define the numbering and sort the numbering size based on the example file of the arithmetic sequence with the first item being 1 and the tolerance being 1.

(3) Read the node temperature corresponding to the Y-shaped region to be combined into the finite element calculation file to complete the extraction of node temperature data.

(4) Move and reassign node temperature data based on welding speed. The size of the grid division in the "Y" - shaped region to be combined will directly affect the number of nodes in the region and the distance between adjacent nodes. The process of node "movement" and re assignment is actually the process of assigning the temperature data of the previous node to the next node by converting it into a certain distance at a known production speed and time.

The establishment process of the heat source model is shown in Fig. 7.

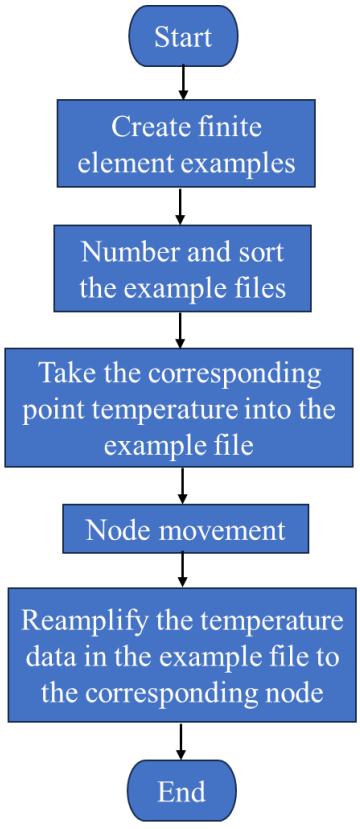

Fig. 7. Flowchart for establishing a heat source model

The temperature distribution along the weld path is shown in Fig. 8.

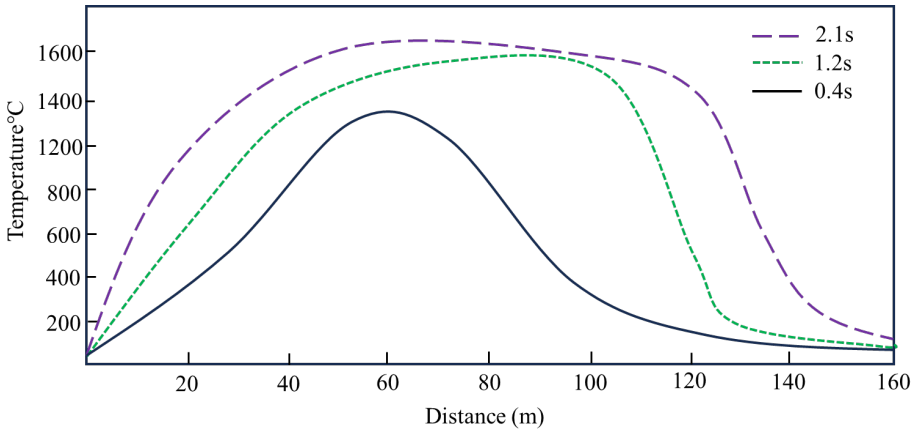

Fig. 8. Temperature dynamic simulation curve

From Fig. 8, it can be seen that the distribution of temperature field on the web under dynamic simulation also shows an increase in the length of the optimal welding area. At the same time, in dynamic simulation, when t = 1.2 seconds, the temperature in the area 50mm to 110mm from the welding end on the web plate reached the Curie temperature. Before reaching the Curie temperature, the temperature rise rate on the steel plate was basically the same. However, before 2.1 seconds, the temperature rise rate on the steel plate was approximately 600 °C/s. In the later stage of induction heating from 1.6 seconds to 2.1 seconds, the temperature rise rate on the steel plate was approximately 153 °C/s. It can be concluded that the temperature rise rate in dynamic simulation is relatively low, which leads to an increase in heating time in state simulation.

4 Prediction Method for Welding Deformation of Chord Beams

Based on SolidWorks simulation data, the relationship between welding parameters and welding deformation is established to address the impact of welding processes on steel welding deformation. With the excellent prediction accuracy and nonlinear generalization ability of BP neural network [15], prediction of welding deformation of chord beams in the previous chapter is achieved, and multiple sets of welding deformations of different sizes of chord beams are predicted.

4.1 Establishment of BP Neural Network Structure

The neural network structure is shown in Fig. 9, where the number of nodes in the input layer and output layer neurons corresponds to the number of feature factors (independent variables) and system objectives (dependent variables), respectively. In the process of predicting the welding deformation of a chord beam in this article, the input variables are gas flow rate, welding current, arc voltage, welding speed, and the output variables are the welding deformation of the chord beam. Meanwhile, due to the different temperature field effects leading to different welding deformations, this article also takes the welding sequence as an input parameter. Therefore, the number of neurons in the input layer is set to 5, and the number of neurons in the output layer is set to 1.

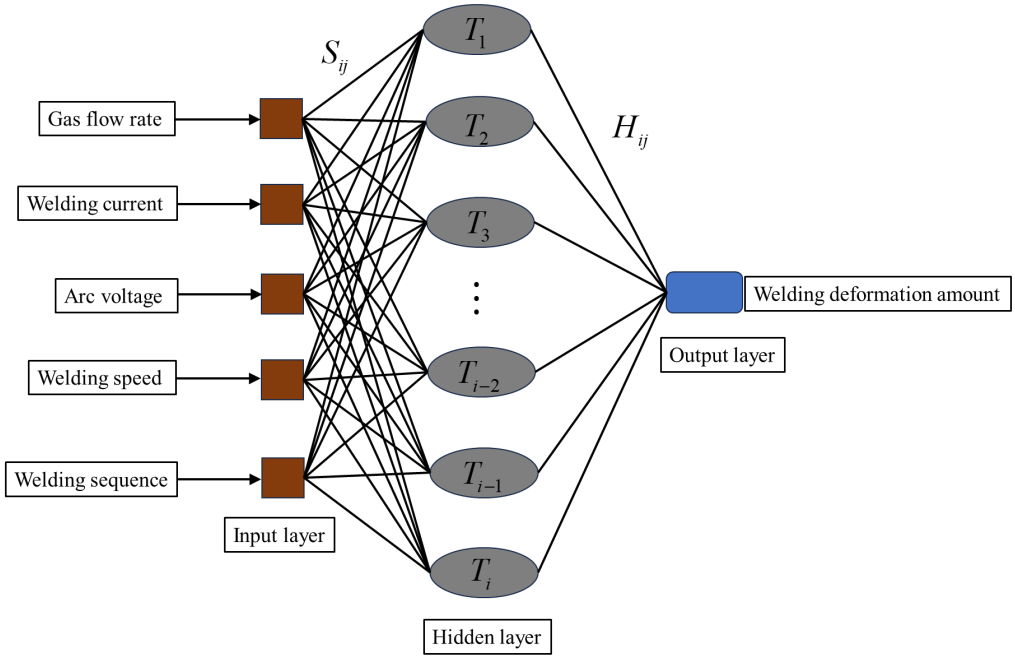

Fig. 9. Triple level neural network structure

In the structure, S_{ij} represents the weight between the j-th hidden layer of the i-th node, and H_{ij} represents the weight between the j-th hidden layer node and the i-th output layer node. For the three-layer structure of the BP neural network, there is a transfer and calculation relationship between the signals in each layer as represented by the following formula, where δ_j represents the threshold from the input layer to the j-th hidden layer node, and ω_k is the threshold from the hidden layer to the k-th output node. The output of the hidden layer node is:

$$Hidden_i = f\left(\sum_{j=1}^{n} s_{ij} h_{ij} - \delta_j\right) = f\left(net_j\right). \tag{13}$$

$$net_j = \sum_{j=1}^{n} s_{ij} h_{ij} - \delta_j. \tag{14}$$

The output formula of the output node is:

$$Out_i = f\left(\sum_{i=1}^{k} s_{ij} h_{ij} - \omega_k\right) = f\left(net_k\right). \tag{15}$$

$$net_j = \sum_{j=1}^{m} s_{ij} h_{ij} - \omega_k. \tag{16}$$

f is called a transformation function:

$$f\left(x\right) = \frac{1}{1+e^{-x}}. \tag{17}$$

The number of hidden layer neurons in the middle is a key parameter that affects the ability of the network model. The method for determining the number of neurons is as follows:

$$k = \sqrt{m + v} + t. \tag{18}$$

In the formula, k represents the number of hidden layer neurons, m represents the number of input layer neurons, v represents the number of output layer neurons, and t represents the adjustable constant.

4.2 Optimization of BP Neural Network Structure

When using the BP neural network directly, this article found that although the BP neural network has the following drawbacks: 1) it is prone to getting stuck in local minima and cannot obtain the global optimal solution; 2) Slow convergence speed and no selection basis for learning rate. 3) The structure of the network is not easy to determine, and a rough range can only be given through empirical formulas. The specific number of hidden layers still needs to rely on multiple experiments. Therefore, this article uses genetic algorithm to improve the neural network in order to achieve satisfactory convergence results.

Genetic algorithm [16] uses genetic space to replace the solution space of actual problems, treating the solution of the problem as a single individual, and then constructs a fitness function based on the needs of the actual problem, and uses the fitness function to calculate the fitness value of each individual. In the process of genetic algorithm operation, each individual's genes may undergo replication, crossover, and mutation, thereby changing the fitness values of their corresponding individuals. With continuous iterative evolution, based on the principles of biological evolution, individuals with good adaptability will be retained, while those with poor adaptability will be eliminated, thus the quality of individuals will become higher and higher.

Genetic algorithm mainly needs to determine the number of weights, thresholds, and fitness values in the neural network. The fitness function reflects the characteristic of genetic algorithm that can search for globally approximate optimal solutions. As the only basis for selection operation, it has a direct impact on the evolutionary operation and convergence speed of genetic algorithm, determining whether the algorithm can find the optimal solution. The form selection of the fitness function in solving different optimization problems is relatively flexible, and the calculation formula is as follows:

$$N = nm + ml + m + l. \tag{19}$$

$$E\left(P_i\right) = \frac{1}{2}\sum_{k=1}^{N}\left(y_{ki} - o_{ki}\right)^2. \tag{20}$$

$$f\left(P_i\right) = \frac{1}{E\left(P_i\right) + a}. \tag{21}$$

n -Number of input layer neurons;
m -The number of hidden layer neurons;
l -The number of hidden layer neurons;
N -Population size;
P_i -Individuals in a population;
o_{ki} -Indicates the expected output of node i on chromosome;
y_{ki} -Indicates actual output;
a -Constant.

According to the above equation, multiple simple experiments were conducted to compare the number of neurons in the intermediate hidden layer during the grid setting process. The experimental results showed that when the number of neurons in the hidden layer was 12, the training error was small and the iteration speed was block. Therefore, the network structure in this paper was set to 5-12-1. The optimization process is shown in Fig. 10.

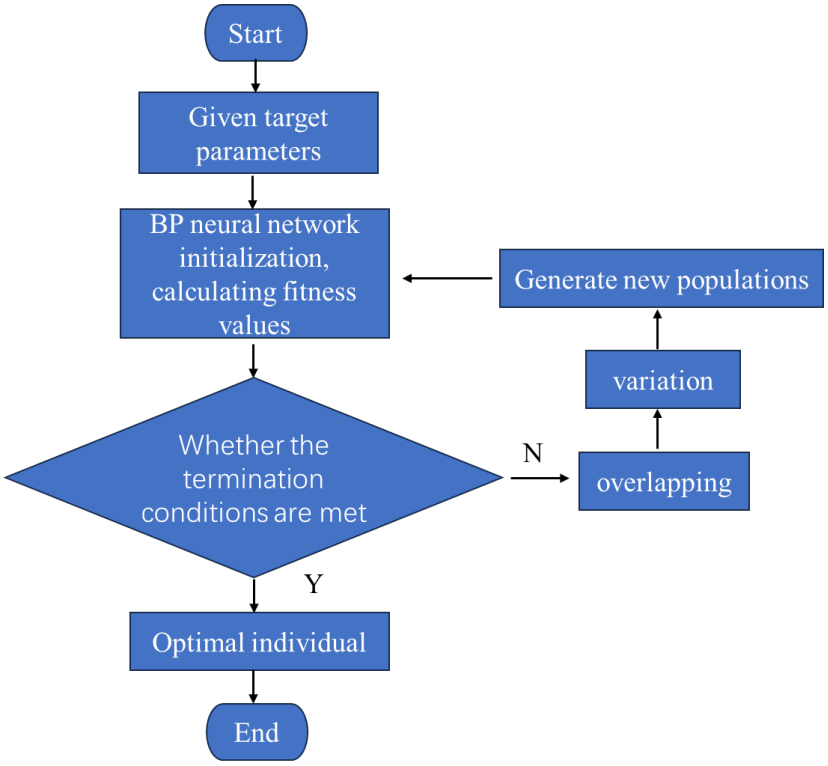

Fig. 10. Algorithm flow chart

The optimized BP neural network is used to predict welding deformation, and the detailed solution process is as follows:

(1) Import the sample set and normalize the training and testing sets in the sample using the selected method.

(2) Based on the actual situation of the problem, construct the topology of the BP neural network and perform pre training to determine the initial weights and threshold lengths.

(3) Population and parameter initialization. Extract randomly selected weights and thresholds from the BP neural network, encode them in real numbers, and form chromosomes in the genetic algorithm.

(4) Selection of fitness function. Determine the fitness function based on the objective function.

(5) Genetic operation, calculating the fitness values of each individual, calculating the probability of each individual based on the fitness values, and selecting individuals with high probability values for crossover and mutation operations. Mutation operation. Using non-uniform variation, a certain gene is randomly perturbed according to the mutation probability m p, and the result of the perturbed changes is used as the new gene value.

(6) Iterative optimization. Determine whether the algebra of genetic evolution satisfies the set relevant parameters. If it does, the genetic algorithm will no longer run and the last generation population will be obtained.

(7) BP neural network training. Decode the optimized optimal value of the genetic algorithm as the optimal weight and threshold of the BP neural network. Train the BP neural network until it reaches the preset accuracy or the maximum number of iterations, and the training ends.

(8) Simulation prediction. Use a trained network model to predict welding deformation results.

5 Simulation Experiments and Result Analysis

Randomly select different parameter combinations from the parameter range in Table 4 for the chord beam welding test. By using the orthogonal transformation method, 120 sets of test data can be obtained, and 120 sets of input data can be obtained. Train and fit the data obtained from the experimental results using a BP neural network Firstly, perform data selection for the neural network: randomly select 100 sets of data from 120 sets of input and output data for network training, and use the remaining 20 sets of data as sample predictions;

Then normalize the data, import it into Matlab, and perform normalization according to the *map* min max() function; Then, use Matlab's built-in *newff* () function to construct a suitable BP neural network; Train a BP neural network using Matlab's built-in train function to train input and output data; Finally, using the built-in sim function in Matlab, the trained BP neural network can predict the output of the function Obtain the prediction and expected output results of the BP neural network, as well as the prediction error results. The results are shown in Fig. 11.

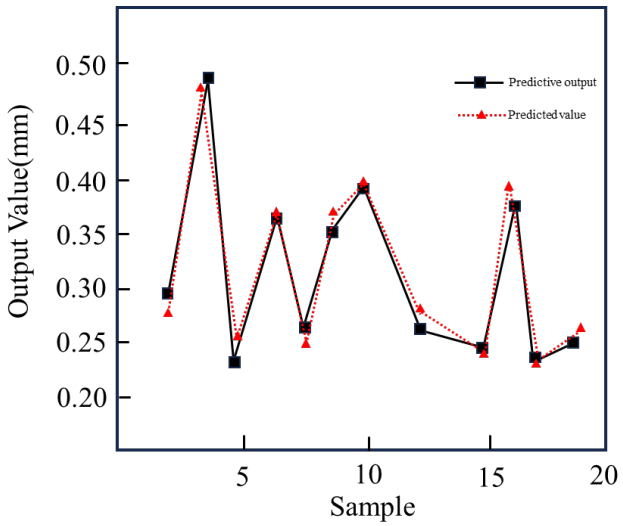

Fig. 11. Fitting results

The comparison between training samples and network learning results is shown in Table 5.

Table 5. Comparison between training sample results and network prediction results

Welding sequence	Welding speed/A	Welding current (mm/s)	Welding deformation/mm	Network prediction results/mm	Relative error (%)
1	280	17	2.27	2.3101	-1.766
1	290	20	1.84	1.8503	0.559
1	300	20	1.97	1.9736	0.182
1	310	17	1.85	1.8421	-0.427
2	280	17	3.21	3.2097	-0.009
2	290	20	1.73	1.7325	0.144
2	300	20	2.36	2.3728	0.542
2	310	17	1.92	1.9132	-0.354
3	280	17	4.93	4.9317	0.034
3	290	20	2.63	2.6303	0.011
3	300	20	3.07	3.0752	0.169
3	310	17	2.95	2.8994	-1.715

After the above comparison, it can be seen that the maximum error of network training is 1.766%, the minimum error is 0.009%, the overall error is small, and the learning state is good. Meanwhile, Table 5 indicates that the error between the predicted and simulated values is relatively small, with a maximum error of 1.766% and a minimum error of 0.009% for the selected predicted data. Therefore, it can be determined that the prediction model based on BP neural network for the influence of gas flow rate, welding current, arc voltage, welding speed, and welding sequence on welding deformation is effective, reliable, and accurate. It realizes the mapping of non-linear relationship between welding parameters and welding deformation, and can provide theoretical guidance for predicting welding deformation of various specifications of medium boxes.

6 Conclusion

This article establishes the finite element and heat source models of the chord beam based on the characteristics of the target object being welded. Then, based on existing data, an improved BP neural network is used to predict welding deformation using input conditions such as welding current, welding speed, and welding sequence. Because BP neural networks themselves have the following characteristics: 1) they are prone to getting stuck in local minima and cannot obtain global optimal solutions; 2) Slow convergence speed and no selection basis for learning rate. 3) The structure of the network is difficult to determine, and there are other shortcomings. This article also elaborates on the optimization process of using genetic algorithm for BP neural network, and constructs a prediction model for BP neural network to improve the prediction process. Finally, a simulation experiment model was built using Matlab simulation software, and the simulation experiment was completed. The predicted results were compared with the actual results, and the maximum error between the predicted and actual values was% 1.766, which met the expected effect.

For the prediction of welding deformation, this article simplified it in Chapter 3.2 to improve the calculation speed of the algorithm. However, in actual operation, it was found that there were deviations in the prediction of deformation. Therefore, the following improvements should be made in further work:

1) Modeling simplified conditions to make the method described in this article more adaptable to the welding environment of beams;

2) For the optimization of BP neural networks, more methods should be adopted to make the comparative results more convincing;

3) Continuously improving solution methods and reducing prediction errors.

References

[1] Y.-D. Fan, Advances in the Welding Procedure and Distortion Control for Aluminum Alloy Longitudinal Beam of Chassis, Fujian Metallurgy 51(4)(2022) 38-42+37.

[2] C.-H. Li, S. Guo, K.-Y. Yang, Welding Numerical Simulation of Joints Between Aluminum Alloy Box Columns and H-Shaped Beams, Industrial Construction 53(8)(2023) 89-95.

[3] M.-T. Huang, G.-P. Liu, Simulation analysis of welding temperature field of the automobile rear based on ANSYS, Woodworking Machinery (1)(2023) 16-18.

[4] B. Li, L. Wang, Y. Liu, F.-D. Wang, Y.-Q. An, Numerical Simulation Analysis for Welding Sequence Optimization of Cabin Frame Structure, Journal of Shenyang Ligong University 42(6)(2023) 69-74+82.

[5] Y.-L. Zhang, Q.-H. He, J.-Y. Zhu, G.-H. Liang, J.-M. Zeng, D.-A. Deng, Prediction of welding deformation in large long straight beams for locomotive, Transactions of the China Welding Institution 44(9)(2023) 106-112+135.

[6] X.-W. Pu, C.-H. Zhang, S. Li, D. Deng, Simulating welding residual stress and deformation in a multi-pass butt-welded joint considering balance between computing time and prediction accuracy, The International Journal of Advanced Manufacturing Technology 93(5)(2017) 2215-2226.

[7] Y. Liu, H.-Y. Li, H.-F. Jiang, Artificial neural network modelling to predict hot deformation behaviour of zinc-aluminium alloy, Materials Science and Technology 41(2)(2013) 214-219.

[8] G.-T. Zhou, Q.-R. Hu, B. Liu, W. Song, Y.-L. Guo, Z.-H. Yu, Assisting controlling of deformation mechanism and stress evolution in high-strength aluminum alloy thin plate welding by trailing hybrid high-speed gas fluid field, Transactions of the China Welding Institution 44(2)(2023) 32-39+131.

[9] H.-L. Gao, G.-X. Liu, Q.-H. Bao, X. Li, Q. Wang, F.-L. Cui, Q.-K. Zhi, P. Zhou, X.-Q. Liu, J. Xu, Research on Boundary Constraints Effect on Welding Residual Stress and Deformation of Bucket Lug, Coal Mine Machinery 43(2)(2022) 29-33.

[10] H.-R. Ju, W. Feng, R.-P. Guo, C.-F. Liu, X.-Y. Tian, G.-Q. Zhuang, J.-F. Zhao, G.-T. Yang, Welding Residual Stress in Butt Weld with Dissimilar Thuckness of Steel Plate, Low Temperature Architecture Technology 44(4)(2022) 86-91+103.

[11] Y.-L. He, X. Qian, X.-W. Ye, Z.-C. Zhang, Finite element analysis of fatigue life of welded joint considering residual stress, Journal of Civil and Environmental Engineering 44(3)(2022) 54-61.

[12] Y. Li, Fatigue Analysis of Front Swingarm based on Solidworks Simulation, Motorcycle Technology (5)(2022) 30-34.

[13] G.-Y. He, T. Wang, Transient finite element three-dimensional numerical model of laser polishing based on moving Gaussian heat source, Laser & Infrared 51(5)(2021) 575-583.

[14] M. Li, J. Cao, Y.-D. Zhou, X.-L. Liu, Research on Numerical Simulation of Double-Belly Crane Beam Welding Process in Nuclear Power Plant, Modern Information Technology 7(7)(2023) 105-110+116.

[15] W. Wang, Construction of Bridge Temperature Prediction Model Based on Different BP Neural Network Models, Scientific and Technological Innovation 34(2022) 157-160.
[16] H.-H. Wang, C. Li, J. Chen, Sliding Mode Control Design and Optimization of Liquid Drive Injector Based on Genetic Algorithm, Machinery Design & Manufacture (6)(2023) 97-100.